Inorganic Chemistry

Article

pubs.acs.org/IC

Blue-Emitting Eu^{2+}-Activated LaOX (X = Cl, Br, and I) Materials: Crystal Field Effect

Donghyeon Kim,[†] Sangha Park,[‡] Sungyun Kim,*[,§] Seong-Gu Kang,[⊥] and Jung-Chul Park*[,†,‡]

[†]Graduate School of Advanced Engineering, Silla University, Busan 617-736, Republic of Korea

[‡]Department of Engineering in Energy & Applied Chemistry, Silla University, Busan 617-736, Republic of Korea

[§]Hoseo University, 165 Sechul Li, Baebang Myun, Asan, Chungnam 336-795, Republic of Korea

[⊥]Department of Chemical Engineering, Hoseo University, Asan-Si, Chungnam-Do 336-795, Republic of Korea

ABSTRACT: Novel blue-emitting LaOBr:Eu^{2+} and LaOI:Eu^{2+} phosphors have been successfully synthesized and compared to LaOCl:Eu^{2+}. The emission spectra of LaOX:Eu^{2+} (X = Cl, Br, and I) show that the peak maxima change somewhat to the red-shift region; 425 nm for LaOCl:Eu^{2+}, 427 nm for LaOBr:Eu^{2+}, and 431 nm for LaOI:Eu^{2+}, which is quite opposite to one based on spectrochemical series (I^- < Br^- < Cl^-). From diffuse reflectance spectra, the band gap energies for LaOCl, LaOBr, and LaOI host lattice are estimated as 5.53 eV (44 594 cm^{-1}), 5.35 eV (43 142 cm^{-1}), and 4.82 eV (38 868 cm^{-1}), respectively, using the Kubelka−Munk function. For LaOX host lattices, the band gap energies are gradually decreased going from Cl to I as the order of energy levels of *n*p orbitals is Cl 3p < Br 4p < I 5p. A quantum wave function calculation from crystal field theory (CFT) indicates the same tendency with experimental data in the LaOX:Eu^{2+} (X = Cl, Br, and I) phosphor materials. With considerations of the radial wave function shape, crystral structure differences and electronegativities among phosphor materials, the splitting energies of 5d orbitals are calculaed; ΔE_{Cl} = 14 597 cm^{-1}, ΔE_{Br} = 14 864 cm^{-1}, ΔE_I = 15 001 cm^{-1} for LaOX:Eu^{2+} (X = Cl, Br, and I). It is noteworthy that the crystal field strength decreases when the interatomic distance decreases, which is probably dependent on the ionic radius of halide ions in the series of LaOX:Eu^{2+} phosphor materials.

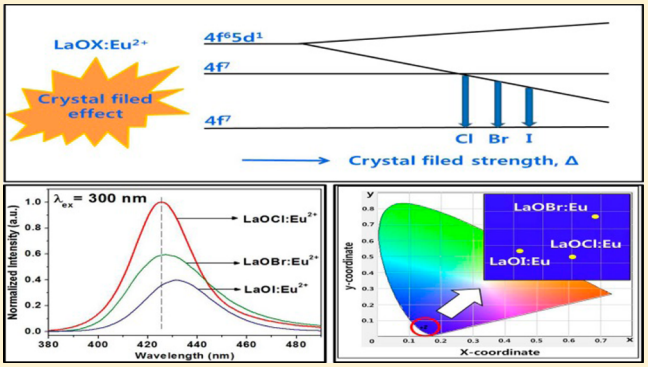

INTRODUCTION

Lanthanide oxyhalide phosphors with various activators, such as Nd^{3+}, Pr^{3+}, Sm^{3+}, Eu^{3+}, Ce^{3+}, Tb^{3+}, and Tm^{3+}, have been of interest for displays, X-ray intensifying screens, and optoelectronic devices.[1−8] More especially, rare-earth oxyhalide phosphors have been considered as a potential candidate material for X-ray image converter devices utilizing luminescent materials. For the application of X-ray image converter, especially in medical radiography, it is necessary that phosphor materials should response rapidly and have high brightness for conversion of the X-rays to visible light. So, lanthanide oxyhalide phosphors have been widely studied for improved luminescent materials with high sensitivity and efficiency to X-rays.[9−11] It is well-known that divalent europium ions (Eu^{2+}) in phosphor materials have been widely used as very important and useful activators that exhibit broad emission bands between ultraviolet (UV) and the red spectral range, corresponding to the $4f^65d^1 \rightarrow 4f^7$ transition.[12−14] We reported, for the first time, a novel blue-emitting Eu^{2+} activated LaOCl phosphor synthesized using the solid-state reaction between La_2O_3 and excess NH_4Cl at 1000 °C under a reducing atmosphere (4% H_2−Ar mixture gas).[15] XRD measurements revealed that the LaOCl:Eu^{2+} polycrystalline particles are well-oriented along the [001] axis above 2.5 mol ratio (mol (NH_4Cl)/mol (La_2O_3)). Photoluminescence (PL) analyses indicated that Eu^{2+} ions are well-stabilized into the La sites in the LaOCl crystal lattice, because PL spectra of the LaOCl:Eu_{2+} phosphor consist of the characteristics of Eu^{2+}.[16−18] Assuming that Cl ions in LaOCl host lattice are replaced with different halide ions, such as Br and I, the luminescent properties of LaOX:Eu^{2+} (X = Br and I) might be changed. Unfortunately, until now, to the best of our knowledge, Eu^{2+}-activated LaOBr and LaOI phosphor materials have not been reported. The LaOX (X = Cl, Br, and I) phases have a tetragonal structure with a D_{4h}^7−*P*4/*nmm* space group (*Z* = 2).[19] The crystal structure of LaOX compounds is composed of layers of similar atoms, that is, a central planar square sheet of oxide ions sandwiched between sheets of Cl^- ions. The La^{3+} ions lie on either side of the central oxygen sheet in distorted square antiprismatic sites and are coordinated to four oxide ions and four Cl^- ions. An additional Cl^- ion in the adjacent layer caps the four-chloride face of the square antiprism.[20] The luminescent property is dependent on the rare earths serving either as an activator or as a host lattice, which plays an important role in phosphor materials. Moreover, the anions (Cl, Br, and I) of the host lattice (lanthanum oxyhalide) could

Received: July 1, 2014
Published: October 30, 2014

   dx.doi.org/10.1021/ic5015576 | *Inorg. Chem.* 2014, 53, 11966−11973

alter the electronic structure of activator ions, which results in the modification of the luminescent properties of lanthanum oxyhalide phosphor materials. The anion ligands, as depicted in Table 1, have very different properties, in particular f-factor values as the nature of the ligands, which is the one of the several factors affecting the extent of splitting of the d orbitals by ligands in crystal field theory (CFT). It should be pointed out that the blue-emitting behaviors of LaOCl:Eu^{2+} phosphors synthesized at 1000 °C under a 4% H_2−Ar atmosphere are associated with the allowed $4f^65d \rightarrow 4f^7$ transitions of Eu^{2+}.[15−18] So, depending on the halide ions, it might be possible to define the variation of the luminescent behaviors in the Eu^{2+}-activated LaOX (X = Cl, Br, and I) phosphor materials. For the study of the crystal field effect in solid crystal structure, lanthanide oxyhalides (REOX) can be regarded as a good reference material providing different halide ligands and activated rare-earth ions. In effect, in the LaOX with PbFCl-type structure, the intralayer La−4X and the interlayer La−X bond length vary considerably, while the La−4O bond length remains almost the same (~2.40 Å). With the larger halides (Cl, Br, and I), the difference between the distance to the four nearest neighbors and to the fifth X neighbor increases considerably, going from LaOCl to LaOI. Coordination field analysis of the fluorescence spectra of LaOX:Eu^{3+} (X = Cl, Br, and I) phosphors was studied using the double-sphere coordination point-charge field model.[22] According to the result, a comparison of the crystal field parameters (B_m^k) along the LaOX:Eu^{3+} (X = Cl, Br, and I) series showed an increase in the strength of the coordination field effect with the increasing ionic radius and the decreasing electronegativity of X^- anions. Crystal field and free-ion analysis for Eu^{3+} ion in the host series of LaOBr−LaOCl−LaOF was reported by Wang et al.,[23] and they mentioned that the crystal field strength decreased along the series of ligands, Br → Cl → F, which is contrary to spectrochemical series. Crystal fields analyses in $La_{1-x}Gd_xOCl:Eu^{3+}$ compounds were performed by Hölsä et al.,[24] and they argued that some local distortions leading to the splitting of the $^7F_1$ doubly degenerated energy level were observed. In previous CFT studies, crystal field parameters were obtained from potential expansion and group symmetries were considered.[22−25] With advances in computer technology, it is now possible to numerically calculate the first-order perturbation integral of each ion in a straightforward manner, without expanding potentials according to group symmetry. It is worthwhile to check how crystal structure differences and wave function shape effects manifest in first-order CFT calculation. In this work, we report on the synthesis and characterization of Eu^{2+}-activated LaOX (X = Cl, Br, and I) phosphor materials. In particular, anionic halides effects are calculated in first-order perturbation and their differences are discussed based on crystal field theory.

Table 1. Properties of Anionic Ligands (Cl, Br, and I)[a]

ligand	electronegativity (Pauling)	ionic radius (Å, CN = 6)	f-factor (in CFT)
Cl	3.16	1.81	0.78
Br	2.96	1.96	0.72
I	2.60	2.20	lower than Br

[a]Data taken from ref 21. CN = coordination number.

EXPERIMENTAL SECTION

The lanthanum oxyhalide phosphors, $La_{1-x}Eu_xOX$ (X = Cl, Br, and I), were prepared from the following solid-state reaction:

$$La_{2-x}Eu_xO_3 + 2NH_4X \rightarrow 2La_{1-0.5x}Eu_{0.5x}OX + 2NH_3 + H_2O \quad (1)$$

The starting materials were a stoichiometric mixture of La_2O_3, Eu_2O_3, and NH_4X. Finely ground mixtures of rare-earth oxides and ammonium halide (excess quantity) were fired at 1050 °C (heating rate = 3 °C min^{-1}) under 4% H_2−Ar for 3 h. For the homogeneous reaction, alumina boats with a cover were used in order to maintain enough collision time between $La_{2-x}Eu_xO_3$ and NH_4X, and to prevent unreacted NH_4X from a rapid outgassing. The structure of LaOX:$Eu_{0.01}$ (X = Cl, Br, and I) was characterized using a X-ray diffractometer (XRD 6000 model, Shimadzu) using Cu Kα radiation at 30 kV and 30 mA. The unit-cell parameters were obtained using a nonlinear least-squares cell refinement program (UnitCell).[26] The elemental analysis for La and Eu was performed by inductively coupled plasma−emission spectroscopy (ICP) with a Labtam 8400 model. Halide ion concentrations in LaOX:Eu (X = Cl, Br, and I) compounds were determined by Volhard's titration.[27] LaOX:Eu powder sample was accurately weighed to ~200 mg into a 100-mL Erlenmeyer flask and 20 mL (excess quantity for halide ion) of 0.0995 mol/L silver nitrate solution was precisely added by pipet, then 20 mL of 1:1 HNO_3 solution (free from NO_xs). After the sample was completely dissolved on a hot plate, the excess Ag^+ solution with AgX precipitate was cooled. The excess Ag^+ was determined by back-titration with standard KSCN solution, using a microburet (5 mL):

$$X^- + Ag^+ \rightarrow AgX + \text{excess } Ag^+ \quad (2)$$

$$\text{excess } Ag^+ + SCN^- \rightarrow AgSCN \quad (3)$$

The end point was detected by adding iron(III) as a ferric alum, which forms a soluble red complex with the first excess of titrant:

$$Fe^{3+} + SCN^- \rightarrow Fe(SCN)^{2-} \quad (4)$$

In these titrations, the AgCl precipitate should be removed by filtration before titrating, because it is more soluble than AgSCN. However, in the case of Br^- and I^-, it is not necessary to remove the precipitate before titrating (but, in our opinion, it is recommendable to remove AgBr and AgI for the detection of an accurate end point). The photoluminescence excitation and emission spectra were collected using a fluorometer (FS-2 model, Scinco) with a 150 W xenon lamp under an operating voltage of 350 V. The reflectance spectra of phosphors were recorded using an ultraviolet−visible (UV-vis) spectrophotometer (Model UV-2600, Shimadzu) with $BaSO_4$ as a reference.

RESULTS AND DISCUSSION

Structural Characterization. The X-ray diffraction (XRD) patterns of LaOX:$Eu^{2+}_{0.01}$ (X = Cl, Br, and I) synthesized at 1050 °C for 3 h under 4% H_2−Ar mixture gas are shown in Figure 1. XRD patterns reveal that the LaOX phases have a tetragonal structure with a D^7_{4h}−$P4/nmn$ space group (Z = 2). Moreover, the LaOX:Eu^{2+} phases show the strongly enhanced intensity of (00l) planes compared to the JCPDS standard patterns, which means that the LaOX:Eu^{2+} phosphor particles are well-oriented along the [001] axis, as reported earlier.[28] It should be mentioned that novel Eu^{2+}-activated LaOBr and LaOI phosphors are successfully synthesized in this experiment. Figure 2 shows the unit-cell parameters (a and c) of tetragonal LaOX:$Eu^{2+}_{0.01}$ (X = Cl, Br, and I) phosphors synthesized at 1050 °C under a reducing atmosphere of a 4% H_2−Ar mixture gas. The alteration of the unit-cell parameter a in the plane of the layer is small (from 4.12 Å to 4.16 Å), compared with the large increase in the unit-cell parameter c perpendicular to the plane

dx.doi.org/10.1021/ic5015576 | Inorg. Chem. 2014, 53, 11966−11973

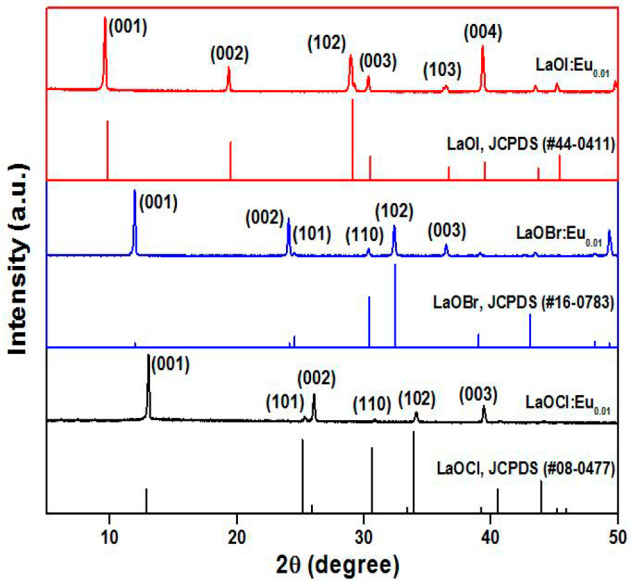

Figure 1. XRD patterns of LaOX:$Eu_{0.01}$ (X = Cl, Br, and I) synthesized at 1050 °C under a 4% H_2−Ar atmosphere for 3 h.

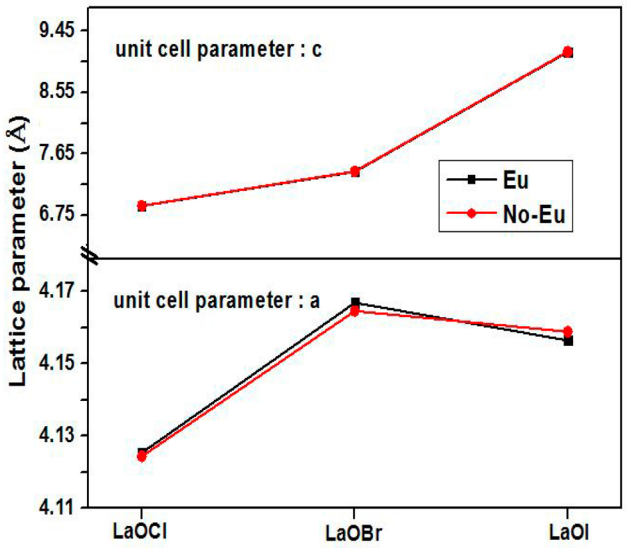

Figure 2. Variation of the unit-cell parameters (*a* and *c*) in LaOX:Eu (X = Cl, Br, and I).

of the layers in the series LaOCl−LaOBr−LaOI (from 6.88 Å to 9.15 Å), which reflects the rigidity of the La_2O_2 system, which consists of a layer of La atoms on each side of an oxygen layer. In the LaOX with PbFCl type structure, the intralayer La−4X and the interlayer La−X bond lengths vary considerably, while the La−4O bond length remains almost the same (~2.40 Å). With the larger halides (Cl, Br, and I), the difference between the distance to the four nearest neighbors and to the fifth X neighbor increases considerably going from LaOCl to LaOI, which results in the 8-coordinated layer structure, especially for LaOI. The interatomic distances in LaOX with the PbFCl structure are indicated in Table 2. As shown in Table 3, elemental analyses using ICP and Volhard's titration reveal that there is no considerable anionic defect in LaOX:Eu^{2+} (X = Cl, Br, and I) phosphor materials. Among several methods for determination of halide ions, it is well-known that ion chromatography has been widely used.[30,31] It

Table 2. Interatomic Distances in LaOX with the PbFCl Structure[a]

	La−4X (Å)	La−X (Å)
LaOCl	3.18	3.14
LaOBr	3.28	3.47
LaOI	3.48	4.79

[a]Data taken from ref 29.

Table 3. Experimental Compositions of LaOX:Eu^{2+} (X = Cl, Br, and I) Determined by Elemental Analyses Using ICP and Volhard's Method

compound	experimental composition[a]	defect concentration
LaOCl:Eu^{2+}	$La_{0.99}Eu_{0.01}OCl_{0.97}$ ($Eu_{0.0095}$, $Cl_{0.972}$)	0.02 Cl
LaOBr:Eu^{2+}	$La_{0.99}Eu_{0.01}OBr_{0.98}$ ($Eu_{0.0089}$, $Br_{0.978}$)	0.01 Br
LaOI:Eu^{2+}	$La_{0.99}Eu_{0.01}O_{0.995}I_{1.00}$ ($Eu_{0.0102}$, $I_{0.998}$)	0.005 O

[a]The La contents are adjusted to be 0.99 by dividing the values obtained using ICP. The contents of Eu and X are obtained by rounding up the third decimal number with the values in parentheses. The O contents are calculated assuming the ideal composition of $La^{3+}_{0.99}Eu^{2+}_{0.01}O^{2-}X^{-1}_{0.99}$.

should be mentioned that Volhard's titration is also a simple and precise one to determine halide ion contents.

Photoluminescence Spectra. The excitation and emission spectra of $La_{1-x}Eu_xOCl$ phosphors, as a function of Eu concentration, are depicted in Figure 3. The PL intensities of LaOCl:Eu phosphors increase as the Eu concentration increases, until the maximum intensity at $x = 0.01$ is observed, then they decrease, because of the concentration quenching. These results reveal that the optimum Eu concentration in the LaOCl:Eu phosphor is ~0.01. Therefore, the optimum Eu concentration is determined as 0.01 in order to examine the effects of halide ions on the luminescent properties in the series of LaOX:Eu^{2+} (X = Cl, Br, and I) phosphor materials. Figure 4 shows the excitation spectra (Figure 4a) and emission spectra (Figure 4b) of LaOX:$Eu_{0.01}$ phosphors synthesized at 1050 °C under a 4% H_2/Ar atmosphere for 3 h. The excitation spectra of LaOX:$Eu_{0.01}$ phosphors (Figure 4a) monitored at wavelength maxima in emission spectra of LaOX:$Eu_{0.01}$ phosphors consist of broad bands between 250 nm and 420 nm, which may be ascribed to the 4f → 5d transition of Eu^{2+}.[16−18] In addition, the highest intensity is observed in the LaOCl:$Eu_{0.01}$ phosphor synthesized at 1050 °C, as shown in the excitation spectra (Figure 4a). The emission spectra (Figure 4b) monitored under the 300 nm excitation show the symmetric bands, but the peak maxima change somewhat to the red-shift region; 425 nm for LaOCl:Eu^{2+}, 427 nm for LaOBr:Eu^{2+}, and 431 nm for LaOI:Eu^{2+}. Compared with the emission ($4f^65d \rightarrow 4f^7$) wavelengths of Eu^{2+} stabilized in some host materials listed in Table 4, it is assured that the differences of the maximum emission wavelength are meaningful in the series of LaOCl:Eu^{2+}−LaOBr:Eu^{2+}−LaOI:Eu^{2+}. For the time being, the origin of the red shift of emission maxima may be due to the different halide ions in LaOX:Eu^{2+} phosphors. As stated above, it is generally accepted that the divalent Eu ions (Eu^{2+}) in phosphor materials exhibit broad emission bands between UV

dx.doi.org/10.1021/ic5015576 | Inorg. Chem. 2014, 53, 11966−11973

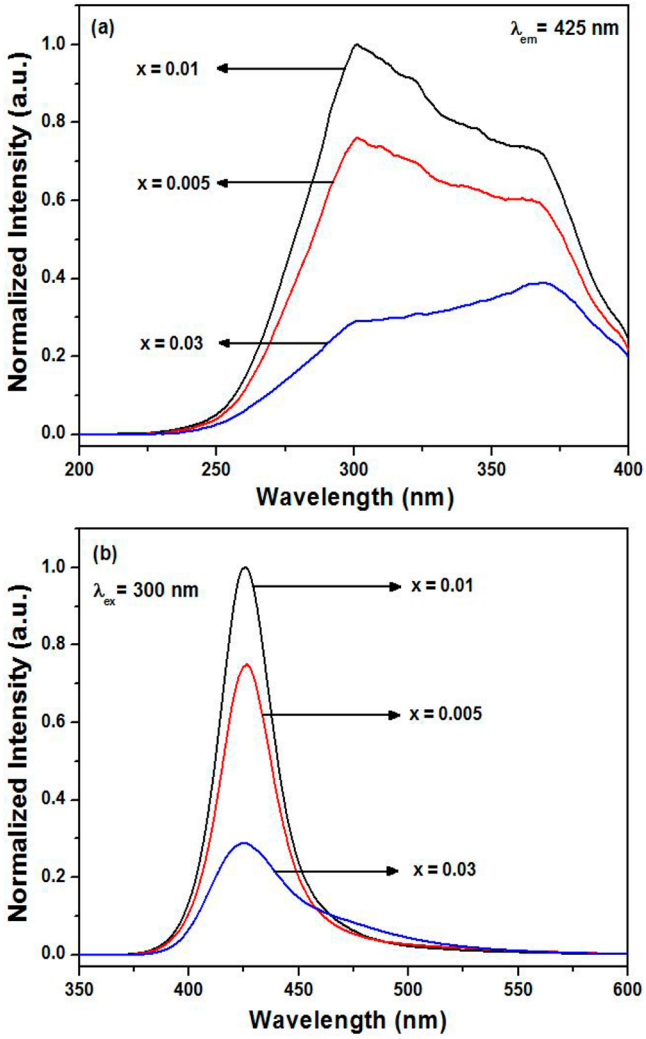

Figure 3. (a) Excitation and (b) emission spectra of $La_{1-x}Eu_xOCl$ synthesized at 1050 °C, as a function of Eu concentration.

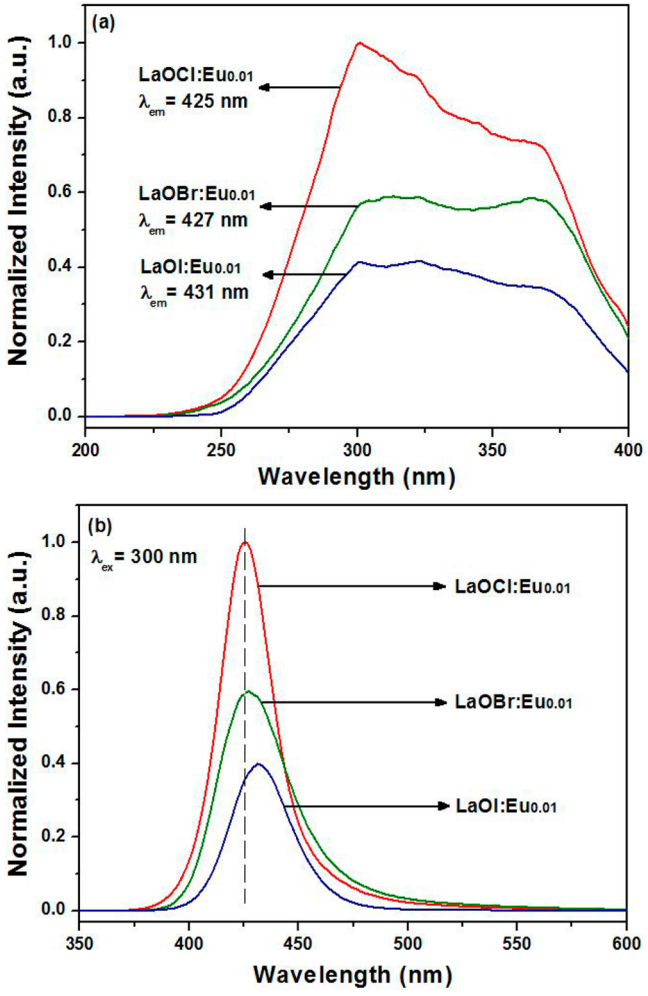

Figure 4. (a) Excitation and (b) emission spectra of $LaOX:Eu_{0.01}$ (X = Cl, Br, and I) synthesized at 1050 °C.

Table 4. Emission ($4f^65d \rightarrow 4f^7$) Wavelengths of Eu^{2+} Stabilized in Some Host Materials

host material	type of host material	λ_{max} (nm)
KCl	single crystal	429 (from ref 32), 427 (from ref 33)
KBr	single crystal	432 (from ref 32), 433 (from ref 33)
KI	single crystal	440 (from ref 32), 438 (from ref 33)
$EuCl_2$	polycrystalline	413 (from ref 34), 416 (from ref 36)
$EuBr_2$	polycrystalline	422 (from ref 35), 420 (from ref 36)
EuI_2	polycrystalline	435 (from ref 36), 440 (from ref 37)

and the red spectral range, corresponding to $4f^65d^1 \rightarrow 4f^7$ transition.[12−14] As depicted in Table 1, the halide ions as the anionic ligands have very different properties. In particular, the f-factor values, which are indicative of the nature of the ligands and are among several factors affecting the extent of splitting of the *d* orbitals by ligands in crystal field theory (CFT), are different; these results are very closely related to the spectrochemical series: $I^- < Br^- < Cl^-$.[21] The strongest crystal field (Cl^-) makes the emission maximum shift to the longest wavelength, and the weakest one (I^-) makes the smallest shift, based on the spectrochemical series. So, one might expect that the order of the emission wavelength is $LaOCl:Eu^{2+}$ > $LaOBr:Eu^{2+}$ > $LaOI:Eu^{2+}$. However, the emission spectra, as shown in Figure 4b, are quite opposite to what we expected, based on the CFT. Figure 5 shows the diffuse reflectance spectra of LaOX and $LaOX:Eu^{2+}$ (X = Cl, Br, and I). When Eu^{2+} ions are doped into the LaOX host lattice, the broad absorption bands are manifested in the range of 250−450 nm. It might be assured that the broad absorption bands at ~250 nm and 450 nm in $LaOX:Eu^{2+}$ phosphors are associated with the $4f^7 \rightarrow 4f^65d$ transition of Eu^{2+} as the absorption bands of the LaOX host lattices are between 200 nm and 250 nm, which is well coincident with the excitation spectra (Figure 4). It should be pointed out that three absorption bands situated at 206 nm (for LaOCl), 222 nm (for LaOBr), and 240 nm (for LaOI) correspond to the valence-to-conduction band transitions of the LaOX host lattices, which may be due to the different halide ions. In order to determine the band-gap energy (E_g) of LaOX host lattices, the diffuse reflectance spectra were transformed using Kubelka−Munk function.[38,39] The inset of Figure 5 shows a band gap of 5.53 eV for LaOCl host lattice. Also, the band gap energies for LaOBr and LaOI host lattice are estimated as 5.35 and 4.82 eV, respectively. It is very interesting that the band-gap energies are gradually decreased going from Cl to I. According to band structure calculations, the filled valence band of LaOX (X = Cl, Br, and I) is mainly of the X−*np* character (*n* = principal quantum number), and the empty conduction band is composed predominantly of La-5d,4f states. For LaOX host lattices, the band gap energies are gradually

dx.doi.org/10.1021/ic5015576 | Inorg. Chem. 2014, 53, 11966−11973

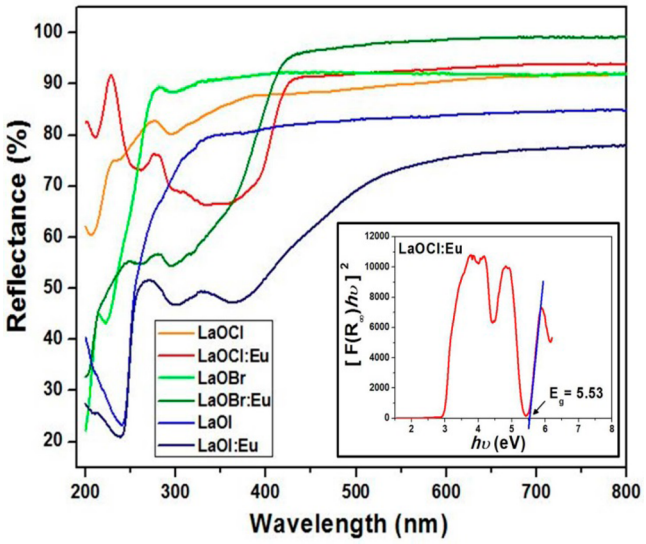

Figure 5. Diffuse reflectance spectra of LaOX and LaOX:Eu^{2+} (X = Cl, Br, and I).

decreased going from Cl to I as the order of energy levels of *np* orbitals is Cl 3p < Br 4p < I 5p. The luminescent behavior of LaOX:Eu^{2+} phosphors were compared with a commercial $(Ca,Sr,Ba,Mg)_5(PO_4)_3Cl:Eu^{2+}$ (CSBM:Eu^{2+}) phosphor (obtained from Nichia Corp., Japan). The excitation and emission spectra of LaOX:Eu^{2+} and CSBM:Eu^{2+} phosphor are shown in Figure 6. The emission spectra under the excitation at 300 nm

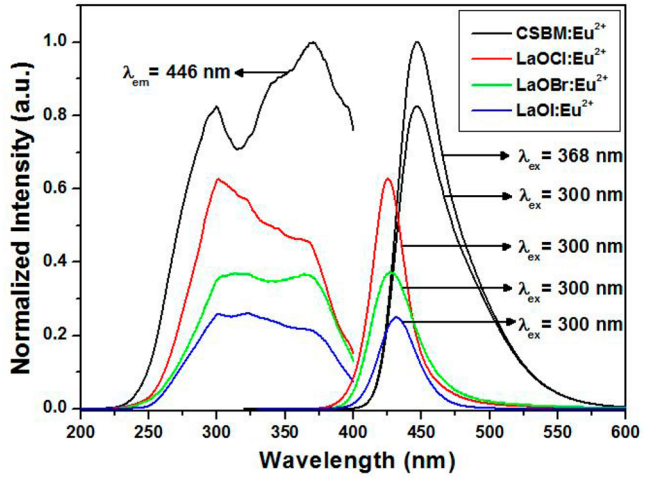

Figure 6. PL spectra of LaOX:Eu^{2+} and a commercial $(Ca,Sr,Ba,Mg)_5(PO_4)_3Cl:Eu^{2+}$(CSBM:$Eu^{2+}$) phosphor.

are somewhat different; for LaOX:Eu^{2+} phosphors, the symmetric emission band centered at ~426 nm with a full width at half maximum (fwhm) of ~30 nm; for CSBM:Eu^{2+} phosphor, the asymmetric band centered at 446 nm with a fwhm of ~50 nm. The difference in the emission spectra between two phosphors may be attributed to the modification of the crystal field around Eu^{2+} due to the different crystal symmetry and constituent atoms. The relative emission intensities of LaOX:Eu^{2+} compared to a commercial CSBM:Eu^{2+} phosphor are ~76% (LaOCl:Eu^{2+}), 45% (LaOBr:Eu^{2+}), and 30% (LaOI:Eu^{2+}).The Commission International de l'Eclairage (CIE) coordinates of LaOX:Eu^{2+} obtained under UV light at 300 nm, are x = 0.151, y = 0.053 (for LaOCl:Eu^{2+}) and x = 0.153, y = 0.064 (for LaOBr:Eu^{2+}), and x = 0.146, y = 0.055 (for LaOI:Eu^{2+}) as shown in Figure 7, which reveals that LaOX:Eu^{2+} compounds are blue-emitting phosphor materials.

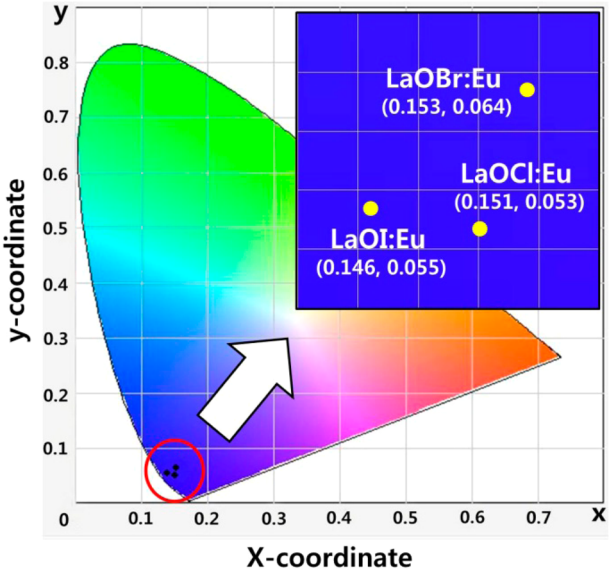

Figure 7. CIE chromaticity for LaOX:$Eu_{0.01}^{2+}$ (X = Cl, Br, and I) monitored under 300 nm UV light.

Theoretical Calculation of Emission Peak Shift. As shown in Figure 4, the emission spectra of LaOX:Eu^{2+} (X = Cl, Br, and I) are quite opposite to the crystal field order. In the spectrochemical series, the crystal field order is I < Br < Cl and a stronger crystal field should make the emission line shift to a longer wavelength, while a weaker one should make a smaller shift.[40] However, experimental data show that LaOI:Eu^{2+} emission has the longest wavelength and LaOBr:Eu^{2+} and LaOCl:Eu^{2+} emission wavelengths are sequentially shorter (these data are also consistent with previous research[41] and Table 4). The order of magnitude of theoretical calculation about emission spectrum differences among LaOCl:Eu^{2+}, LaOBr:Eu^{2+}, and LaOI:Eu^{2+} is presented based on CFT. We only consider the emission energy differences due to splitting and observe their order. The emission spectra are typical and characteristic of the $4f^65d \rightarrow 4f^7$ transition of the Eu^{2+} activator ion. After the Eu^{2+} ion absorbs a photon, one electron is excited to the 5d orbital. After electron excitation, the ion nucleus might relax. The excited electron decays and emits a photon. From the Franck–Condon principle, we may assume that the nucleus remains in the same position during emission.[40] According to CFT, nearby anions split the 5d energy level and the excited electron decays from the split lowest 5d energy level, so the emission energy changes to approximately

$$E_{\text{emission}} \rightarrow E_{\text{emission}} - 0.5\Delta E_{\text{splitting}} \quad (5)$$

The Eu atom has an electron configuration of $[Xe]4f^76s^2$, so the excited Eu^{2+} has the $[Xe]4f^65d^1$ configuration. The approximate Hamiltonian for the outermost $5d^1$ electron wave function then becomes

$$H = H_0 + H_C + H_{LS} \quad (6)$$

where H_0 is the Hamiltonian for central charge plus one outermost electron, H_C represents the nearby ion terms for

dx.doi.org/10.1021/ic5015576 | Inorg. Chem. 2014, 53, 11966–11973

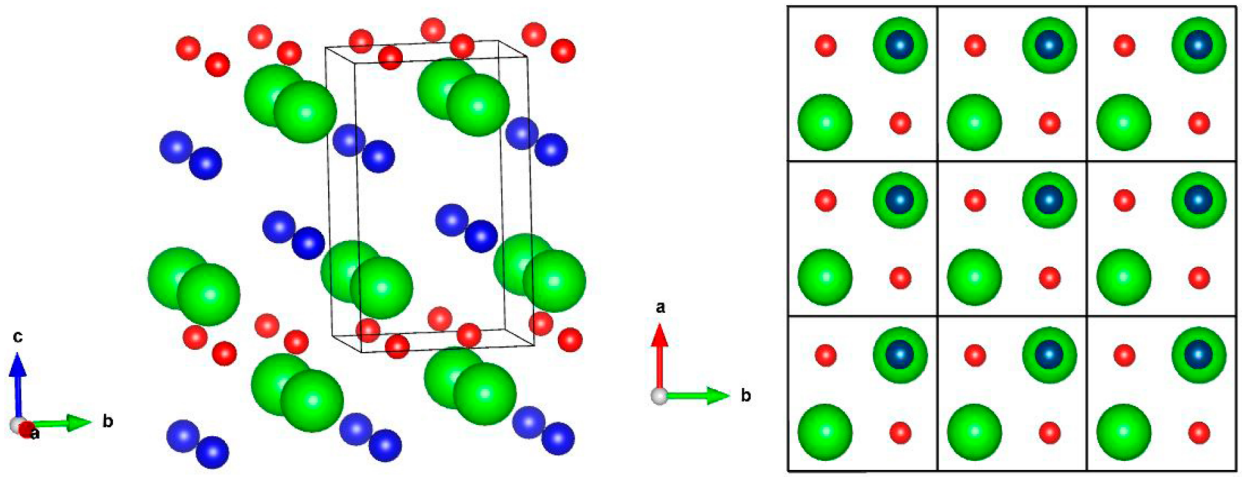

Figure 8. LaOCl structure. Green dots are La atoms, smaller blue dots are Cl atoms, and red dots are O atoms.

crystal field calculation, and H_{LS} is the spin−orbit coupling term. Unperturbed Hamiltonian is set as H_0, and other terms are treated as perturbation. Among perturbation terms, only H_C is dependent on the host lattice, so perturbation from H_{LS} is not needed when the differences among different host lattices are considered. The explicit forms of H_0 and H_C are given as

$$H_0 = -\frac{\hbar^2}{2\mu}\nabla^2 + \frac{Z_c e^2}{r} \qquad H_C = \sum_i \frac{z_i e^2}{|\vec{R}_i - \vec{r}|} \tag{7}$$

where Z_c is the effective central charge (Eu), μ the reduced mass, Z_i the charge number of the ith ion, and $\vec{R}i$ the position vector of the ith ion. H_0 has the same form as the hydrogen wave function Hamiltonian, except for the central charge. The effective charge numbers Z_c and Z_i are determined with electronegativity and anion defect considerations. The electronegativity is a measure of the tendency of an atom in a molecule to attract electrons.[42] With the assumption that an electron wave function in a bonding is part ionic and part covalent, the wave function form is written as $\psi_{molecule} = a\psi_{covalent} + b\psi_{ionic}$ and how much (percentage) of the wave function is covalent and how much (percentage) is ionic is estimated. The following empirical formula[42] for percentage of ionic character is given for two atoms with Pauling electronegativity χ_A and χ_B:

$$\%\ \text{of ionic character} = 16|\chi_A - \chi_B| + 3.5|\chi_A - \chi_B|^2 \tag{8}$$

For covalent bonds, the electron is shared between atoms and for ionic bonds, the electron is transferred to one atom. Therefore, effective charges are calculated by 0.5 (% of covalent character) + (% of ionic character). The Pauling electronegativities are 1.1, 1.2, 3.44, 3.16, 2.96, and 2.66 for La, Eu, O, Cl, Br, and I, respectively. Next, the anion defect of the LaOX:Eu crystal is considered. For LaOCl:Eu, LaOBr:Eu, and LaOI:Eu, the elemental analysis yields, La(0.99) Eu(0.01) O(1.00) Cl(0.972) for LaOCl:Eu, La(0.99) Eu(0.01) O(1.00) Br(0.978) for LaOBr:Eu, and La(0.99) Eu(0.01) O(0.996) I(0.998) for LaOI:Eu. With these data, effective charges are estimated, as follows:

- For LaOCl:Eu, effective charges are +2.3051e (La), −1.5661e (O near La), −1.5340e (O near Eu), −0.7390e (Cl near La), −0.7240e (Cl near Eu).
- For LaOBr:Eu, effective charges are +2.2754e (La), −1.5661e (O near La), −1.5340e (O near Eu), −0.70934e (Br near La), −0.6950e (Br near Eu).
- For LaOI:Eu, effective charges are +2.2334e (La), −1.5661e (O near La), −1.5340e (O near Eu), −0.6673e (I near La), −0.6541e (I near Eu).
- The effective central charge for the outermost Eu^{2+} electron is 2.534e.

For anion defects, random defects are assumed and each element ratio from elemental analysis was multiplied by the effective charges. The eigenfunction of H_0 is written as

$$\langle nlm|r\theta\phi\rangle = R_{nl}(r)Y_{lm}(\theta, \phi)$$

where r is the radial distance, and θ and ϕ are two angles in spherical coordinate; n, l, and m are the principal, angular, and magnetic quantum numbers. $R_{nl}(r)$ and $Y_{lm}(\theta,\phi)$ are referenced as radial and angular wave functions, and their explicit forms for the 5d orbital ($n = 5$, $l = 2$) are

$$R_{52}(r) = 1.2866 \times 10^{35} \exp(-9.5772 \times 10^9 r) r^2 \times [1 - (6.38477 \times 10^9) r + 8.7354 \times 10^{18} r^2] \quad \text{(MKS units)} \tag{9}$$

$$Y_{2m}(\theta, \phi) = \frac{1}{2}\sqrt{\frac{5(2-m)!}{\pi(2+m)!}} \exp(im\phi) P_2^m(\cos\theta) \tag{10}$$

where r is given in meters and P_2^m is the associated Legendre polynomial of (2, m). The energy splitting due to the crystal field is calculated in first-order perturbation as the difference between maximum and minimum of $\langle 5,2,m|H_C|5,2,m\rangle$. To determine the explicit form of H_C, each crystal structure of host lattice is considered as shown in Figure 8. In the LaOX:Eu (X = Cl, Br, I) structure,[29,43,44] the Eu atom occupies the La site. Considered anions and cations near Eu (according to Figure 8) are: O(×4) atoms below La layer, X(×4) atoms in adjacent upper X layer, X(×1) atom in next adjacent upper X layer, X(×1) atom in lower X layer below O layer and La layer, La(×4) atoms in lower La layer below O layer, La(×4) atoms in the same La layer. The distances from Eu ion, in the above order, are 2.338, 3.206, 3.127, 3.756, 3.785, and 4.120 Å for LaOCl; 2.398, 3.283, 3.466, 3.892, 3.797, and 4.145 Å for LaOBr; and 2.410, 3.477, 4.791, 4.335, 3.829, and 4.144 Å for LaOI. The aforementioned data show that each crystal has a

dx.doi.org/10.1021/ic5015576 | Inorg. Chem. 2014, 53, 11966−11973

unique structure. For LaOCl, the nearest Cl atom is the one in next adjacent Cl layer; however, for LaOBr, the nearest Br(×4) atoms are in the adjacent Br layer. For LaOI, the I atom in the next adjacent upper I layer is located farther away than the nearby La(×8) atoms. For consistent comparison of crystal field effects among LaOX:Eu materials, all above anions and cations were included in CFT calculations. The shape of the radial wave function also plays a role. The radial wave function is more important than the angular wave function, in that the radial wave function determines the overall probability density, principal quantum number, and the electron energy. When the excited 5d (Eu^{2+}) electron wave function is calculated in the H-atom-like model, its radial wave function spread widely. With electronegativity consideration, the spread becomes wider. The amplitude of the radial wave function decays abruptly with r, as shown in Figure 9, but Figure 10 shows that the probability of being outside (r > 5 Å) is larger than being inside. This implies that, in perturbation calculation, the effect of ions farther away cannot be ignored. As previously explained in the LaOI:Eu case, the distance of some anions near Eu is larger than those of cations. For consistent perturbation calculation and comparison between LaOX:Eu emission, all atoms inside this distance should be included. Three-dimensional (3D) coordinates of ions can be obtained from crystal data[43] and straightforward numerical calculation of $\langle 5,2,m|H_C|5,2,m\rangle$ is possible, rather than considering crystal parameters by potential expansion and group properties. In our case, La(×8) atoms, O(×4) atoms, and X(×6) atoms are included in numerical calculation. Energy splitting calculation yields

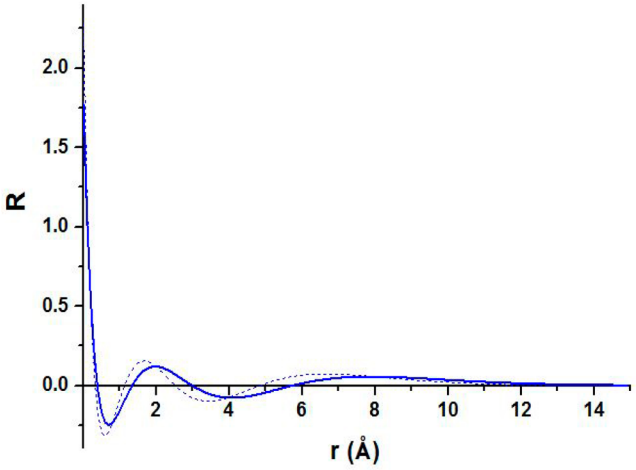

Figure 9. Radial wave function versus r. Dashed line (---) is the radial wave function with a central charge of +3e (without electronegativity consideration); solid line (—) is the wave function with a central charge of +2.534 e (with electronegativity consideration). Wave functions are not normalized.

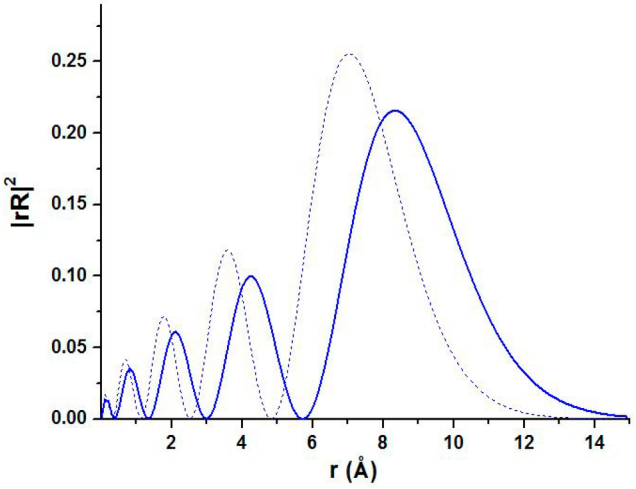

Figure 10. Probability density (integrated over spherical surface) versus r. Dashed line (---) is the radial wave function with a central charge of +3e (without electronegativity consideration); solid line (—) is the wave function with a central charge of +2.534 e (with electronegativity consideration). Smaller central charge gives wider spreading.

$$\Delta E_X = \langle 5,2,m|H_C|5,2,m_{max}\rangle - \langle 5,2,m|H_C|5,2,m_{min}\rangle \quad (11)$$

$$\Delta E_{Cl} = 14597\ cm^{-1}\ (22292\ cm^{-1})$$

$$\Delta E_{Br} = 14864\ cm^{-1}\ (23003\ cm^{-1})$$

$$\Delta E_I = 15001\ cm^{-1}\ (25553\ cm^{-1}) \quad (12)$$

Here, the values inside the parentheses are without electronegativity and vacancy considerations. From eq 5, if the emission energy of host lattice LaOX1:Eu is E_{X1}, then $-0.5(\Delta E_{X1} - \Delta E_{X2})$ should be the theoretical emission energy differences $E_{X1} - E_{X2}$. The experimental emission energy of LaOCl:Eu, LaOBr:Eu, and LaOI:Eu and their differences are

$$E_{Cl} = 23529\ cm^{-1}$$

$$E_{Br} = 23419\ cm^{-1}$$

$$E_I = 23202\ cm^{-1} \quad (13)$$

$$E_{Cl} - E_{Br} = 110\ cm^{-1}$$

$$E_{Br} - E_I = 217\ cm^{-1} \quad (14)$$

In comparison, the theoretical results are

$$-0.5(\Delta E_{Cl} - \Delta E_{Br}) = 134.0\ cm^{-1}\ (335.7\ cm^{-1})$$

$$-0.5(\Delta E_{Br} - \Delta E_I) = 68.5\ cm^{-1}\ (1274.7\ cm^{-1}) \quad (15)$$

(Again, values shown inside parentheses are without electronegativity and vacancy considerations.)

It should be pointed out that the difference of the magnitude of emission energy between experimental and theoretical estimation should not be directly compared, because there are many factors affecting the emission properties in actual phosphor materials, such as the concentration of activator ions, the loss of transferred energy, and the degree of defects. But even with these many other factors, comparison with the experimental emission data show these calculated splitting energies have the same decreasing tendency of emission energy along the series of ligands I → Br → Cl in LaOX:Eu^{2+} phosphor materials, and consideration of electronegativity and vacancies improves the theoretical estimations significantly. It shows that different crystal structures can yield different results from general spectrochemical series expectations.

■ CONCLUSIONS

Novel blue-emitting LaOBr:Eu^{2+} and LaOI:Eu^{2+} phosphors have been successfully synthesized using a solid-state reaction between La_2O_3 and NH_4X (X = Br and I) and compared to

dx.doi.org/10.1021/ic5015576 | Inorg. Chem. 2014, 53, 11966−11973

LaOCl:Eu^{2+}. In the LaOX with PbFCl type structure, the intralayer La−4X and interlayer La−X bond lengths vary considerably, while the La−4O bond length remains almost the same (~2.40 Å). With the larger halides (Cl, Br, and I), the difference between the distance to the four nearest neighbors and to the fifth X neighbor increases considerably going from LaOCl to LaOI, which results in the 8-coordinated layer structure for especially LaOI. The emission spectra monitored under the 300-nm excitation show the symmetric bands, but the peak maxima change somewhat to the red shift region; 425 nm for LaOCl:Eu^{2+}, 427 nm for LaOBr:Eu^{2+}, and 431 nm for LaOI:Eu^{2+}. Compared with the emission ($4f^6 5d \rightarrow 4f^7$) wavelengths of Eu^{2+} stabilized in some host materials, it is assured that the differences of the maximum emission wavelength are meaningful in the series of LaOCl:Eu^{2+}−LaOBr:Eu^{2+}−LaOI:Eu^{2+}. In the spectrochemical series, the crystal field order is I < Br < Cl, so stronger crystal field should make the emission line shifted to longer wavelength, and weaker one should make smaller shift. However, the experimental data show that LaOI:Eu emission has the longest wavelength and LaOBr:Eu and LaOCl:Eu emission wavelengths are sequentially shorter. Crystal field theory (CFT) calculation by quantum wave function with each crystal structure, anion defects and electronegativity considerations also indicates the tendency of experimental data opposite to the spectrochemical series in the LaOX:Eu^{2+} phosphor materials. The energy splitting due to crystal field is calculated in first-order perturbation as the difference between the maximum and the minimum of $\langle 5,2,m|H_C|5,2,m\rangle$. The splitting energies of 5d orbitals are calculated: ΔE_{Cl} = 14 597 cm^{-1}, ΔE_{Br} = 14 864 cm^{-1}, ΔE_I = 15 001 cm^{-1} for LaOX:Eu^{2+} (X = Cl, Br, and I), opposite to the spectrochemical series. Comparing with the experimental emission data, we can see that these calculated splitting energies show the same decreasing tendency of emission energy along the series of ligands, I → Br → Cl in LaOX:Eu^{2+} phosphor materials. It is noteworthy that the crystal field strength decreases when the interatomic distance decreases, which probably depends on the ionic radius of halide ions in the series of LaOX:Eu^{2+} phosphor materials.

AUTHOR INFORMATION

Corresponding Authors

*E-mail: rdecay@gmail.com (S. Kim).
*E-mail: parkjc@silla.ac.kr (J.-C. Park).

Notes

The authors declare no competing financial interest.

REFERENCES

(1) Yi, G.; Sun, B.; Yang, F.; Chen, D.; Zhou, Y.; Cheng, J. *Chem. Mater.* **2002**, *14*, 2910.
(2) Duntelle, G.; Mortier, M.; Vivien, D.; Patriarche, G. *Chem. Mater.* **2005**, *17*, 2216.
(3) Sivakumar, S.; van Veggel, F. C. J. M.; Raudsepp, M. *J. Am. Chem. Soc.* **2005**, *127*, 12464.
(4) Starick, D.; Golovkova, S. I.; Gurvic, A. M. *J. Lumin.* **1982**, *129*, 1552.
(5) Swindells, F. E. *J. Electrochem. Soc.* **1954**, *101*, 415.
(6) Blasse, G.; Bril, A. *J. Chem. Phys.* **1967**, *46*, 2579.
(7) Rambadu, U.; Balaji, T.; Buddhudu, S. *Mater. Res. Bull.* **1995**, *30*, 891.
(8) Lee, S. S.; Park, H. I.; Joh, C. H.; Byeon, S. H. *J. Solid State Chem.* **2007**, *180*, 3529.
(9) Buchanan, R. A.; Maple, T. G.; Sklensky, A. F. (Lockheed Missiles & Space Company, Inc.). U.S. Patent No. 4,297,584, Oct. 27, 1981.
(10) Rabatin, J. *J. Electrochem. Soc.* **1982**, *129*, 1552.
(11) Starick, D.; Golovkova, S. I.; Gurvic, A. M. *J. Lumin.* **1988**, *40*, 199.
(12) Stefani, R.; Maia, A. D.; Teotonio, E. E. S.; Monteiro, M. A. F.; Felinto, M. C. F. C.; Brito, H. F. *J. Solid State Chem.* **2006**, *179*, 1086.
(13) Piao, X.; Horikawa, T.; Hanzawa, H.; Machida, K. *Appl. Phys. Lett.* **2006**, *88*, 161908.
(14) Im, W. B.; Kim, Y. K.; Jeon, D. Y. *Chem. Mater.* **2006**, *18*, 1190.
(15) Kim, D.; Jang, J.; Ahn, S. I.; Kim, S. H.; Park, J. C. *J. Mater. Chem. C* **2014**, *2*, 2799.
(16) Zhang, S.; Nakai, Y.; Tsuboi, T.; Huang, Y.; Seo, H. J. *Chem. Mater.* **2011**, *23*, 1216.
(17) Im, W. B.; Kim, Y. I.; Yoo, H. S.; Jeon, D. Y. *Inorg. Chem.* **2009**, *48*, 557.
(18) Inoue, K.; Hirosaki, N.; Xie, R. J.; Takeda, T. *J. Phys. Chem. C* **2009**, *113*, 9392.
(19) Templeton, D. H.; Dauben, C. H. *J. Am. Chem. Soc.* **1953**, *75*, 6069.
(20) Whittingham, M. S.; Jacobson, A. J. *Intercalation Chemistry*; Academic Press: New York, London, 1982.
(21) Huheey, J. E.; Keiter, E. A.; Keiter, R. L. *Inorganic Chemistry: Principles of Structure and Reactivity*; Harper Collins College Publishers: New York, 1993.
(22) Yang, P.; Li, S.; Wang, Y. *J. Phys.: Condens. Matter* **1991**, *3*, 483.
(23) Wang, Q.; Gao, Y.; Bulou, A. *J. Phys. Chem. Solids* **1995**, *56*, 285.
(24) Hölsä, J.; Koski, K.; Lamminäki, R.-J.; Säilynoja, E.; Dereń, P.; Stręk, W. *J. Alloys Compd.* **1997**, *250*, 370.
(25) Hölsä, J.; Porcher, P. *J. Chem. Phys.* **1982**, *78*, 6.
(26) Holland, T. J. B.; Redfern, S. A. T. *J. Appl. Crystallogr.* **1997**, *30*, 84.
(27) Christian, G. D. *Analytical Chemistry*; John Wiley & Sons: Hoboken, NJ, 2004.
(28) Afanasier, P.; Aouine, M.; Deranlot, C.; Epicier, T. *Chem. Mater.* **2010**, *22*, 5411.
(29) Wyckoff, R. W. G. *Crystal Structure*; Interscience: New York, 1963.
(30) Mehra, M. C.; Pelletier, C.; Tardif, D. *Asian J. Chem.* **1990**, *2*, 331.
(31) Wang, L. H. *J. Chromatogr. Sci.* **2002**, *40*, 326.
(32) Muñoz Santiuste, J. E.; García Solé, J. *Phys. Rev. B* **1990**, *42*, 11339.
(33) Zaldo, C.; Calleja, J. M.; Orozco, M. E. *J. Phys. C: Solid State Phys.* **1987**, *20*, 849.
(34) Brixner, L. H.; Bierlein, J. D. *Mater. Res. Bull.* **1974**, *9*, 99.
(35) Machida, K. I.; Adachi, G. Y.; Yasuoka, N.; Kasai, N.; Shiokawa, J. *Inorg. Chem.* **1980**, *19*, 3807.
(36) Brixner, L. H. *Mater. Res. Bull.* **1976**, *11*, 269.
(37) Wang, L.; Wang, S.; Zhao, X.; Sun, J. *J. Alloys Compd.* **1995**, *225*, 174.
(38) Kotüm, G. *Reflectance Spectroscopy*; Springer−Verlag: New York, 1969.
(39) Tandon, S.; Gupta, J. *Phys. Status Solidi* **1970**, *38*, 363.
(40) Shionoya, S.; Yen, W. M. *Phosphor Handbook*; CRC Press: Boca Raton, FL, 1999.
(41) P. Dorenbos, P. *J. Lumin.* **2003**, *104*, 239.
(42) House, J. E. *Inorganic Chemistry*; Elsevier: Amsterdam, 2008.
(43) http://www.crystallography.net/.
(44) Maslen, E. N.; Streltsov, V. A.; Streltsova, N. R.; Ishizawa, N. *Acta Crystallogr., Sect. B: Struct. Sci.* **1996**, *52*, 576.